Independent Component Analysis For EEG Source Localization In Realistic Head Models

Leonid Zhukov, David Weinstein and Chris Johnson
Center for Scientific Computing and Imaging
University of Utah

Abstract—

A pervasive problem in neuroscience is determining which regions of the brain are active, given voltage measurements at the scalp. If accurate solutions to such problems could be obtained, neurologists would gain non-invasive access to patient-specific cortical activity. Access to such data would ultimately increase the number of patients who could be effectively treated for neural pathologies such as multi-focal epilepsy.

However, estimating the location and distribution of electric current source within the brain from electroencephalographic (EEG) recordings is an ill-posed problem. Specifically, there is no unique solution and solutions do not depend continuously on the data. The ill-posedness of the problem makes finding the correct solution a challenging analytic and computational problem.

In this paper we consider a spatio-temporal method for sources localization, taking advantage of the entire EEG time series to reduce the configuration space we must evaluate. The EEG data is first decomposed into signal and noise subspaces using a Principal Component Analysis (PCA) decomposition. This partitioning allows us to easily discard the noise subspace, which has two primary benefits: the remaining signal is less noisy, and it has lower dimensionality. After PCA, we apply Independent Component Analysis (ICA) on the signal subspace. The ICA algorithm separates multichannel data into activation maps due to temporally independent stationary sources. For each activation map we perform an EEG source localization procedure, looking only for a single dipole per map. By localizing multiple dipoles *independently*, we substantially reduce our search complexity and increase the likelihood of efficiently converging on the correct solution.

Keywords: EEG, ICA, PCA, source localization, realistic head model

Introduction

Electroencephalography (EEG) is a technique for the non-invasive characterization of brain function. Scalp electric potential distributions are a direct consequence of internal electric currents associated with neurons firing and can be measured at discrete recording sites on the scalp surface over a period of time.

Most measured, non-background brain activity is generated within the cerebral cortex, the outer surface (1.5-4.5 mm thick) of the brain comprised of approximately ten billion neurons. The active regions within the cortex are generally fairly well localized, or *focal*. Their activity is the result of synchronous synaptic stimulation of a very large number ($10^5 - 10^6$) of neurons. Cortical neurons align themselves in columns oriented orthogonally to the cortical surface [1]. When a large group of such neurons all depolarize or hyperpolarize in concert, the result is a dipolar current source oriented orthogonal to the cortical surface. It is the propagation of this current that we measure using EEG.

Estimation of the location and distribution of current sources within the brain based on potential recordings from the scalp (source localization) is one of the fundamental problems in electroencephalography. It requires the solution of an inverse problem, i.e., given a subset of electrostatic potentials measured on the surface of the scalp, and the geometry and conductivity properties within the head, calculate the current sources and potential fields within the cerebrum. This problem is challenging because solutions do not depend continuously on the data and because it lacks a unique solution.[1] The lack of continuity implies that small errors in the measurement of the voltages on the scalp can yield unbounded errors in the recovered solution. The non-uniqueness is a consequence of the linear superposition of the electric field: different internal source configurations can produce identical external electromagnetic fields, especially when only measured at a finite number of electrode positions [1], [3], [4].

However, if accurate solutions to such problems could be obtained, neurologists would gain non-invasive access to patient-specific cortical activity. Access to such data would ultimately increase the number of patients who could be effectively treated for pathological cortical conditions such as epilepsy [5], [6].

There exist several different approaches to solving the source localization problem. Initially, many of these were implemented on spherical models of the head [7], [8]. Those methods that proved promising were then extended to work on realistic geometry [9]. One of the most general methods for inverse source localization involves starting from some initial distributed estimate of the source and then recursively enhancing the strength of some of the solution elements, while decreasing the strength of the rest of the solution elements until they become zero. In the end, only a small number of elements will remain nonzero, yielding a localized solution. This method is implemented, for example, in the FOCUSS algorithm [10]. Another example of an iterative re-weighting technique is the LORETA algorithm [11].

A second source localization approach incorporates *a priori* assumptions about sources and their locations in the model. Electric current dipoles are usually used as sources, provided that the regions of activations are relatively fo-

[1] Mathematically, problems fitting such a profile are termed ill-posed [2].

cused [3]. Although a single dipole is the most widely used model, it has been demonstrated that a multiple dipole model is required to account for a complex field distribution on the surface of the head [12]. If the distance between the dipoles is large or the dipoles have entirely different temporal behavior, the field patterns may exhibit only minor overlap and they can be fit individually using the single-dipole model. However, more often than not, examination of spatial surface topographies can be misleading, as the time series of multiple dipoles overlap and potentials cancel each other out [4], [13]. In such cases, one must employ a third approach: a spatio-temporal model.

The main assumption of this model is that there are several dipolar sources that maintain their position and orientation, and vary just their strength (amplitude) as a function of time. Now, rather than fit dipoles to measurements from one instant in time, dipoles are fit by minimizing the least-square error residual over the entire evoked potential epoch [14].

A more advanced version of this spatio-temporal approach is developed in the multiple signal classification algorithm, MUSIC [15], and in its extension, RAP-MUSIC [16]. A signal subspace is first estimated from the data and the algorithm then scans a single dipole model through the three-dimensional head volume and computes projections onto this subspace. To locate the source, the user must search the head volume for local peaks in the projection metric. The RAP-MUSIC extension of this algorithm automates this search, extracting the location of the sources through a recursive use of subspace projection.

While the above methods represent significant advances in source localization, they fail to address the problem most recently identified by Cuffin in [17]: "Solutions to multiple dipole ... sources are much less reliable than solutions for single-dipole sources. These solutions can be very sensitive to ... noise. At present, this sensitivity limits the usefulness of these solutions as clinical and research tools." In this paper, we introduce a novel approach for spatio-temporal source localization of *independent* sources. In our method, we first separate the raw EEG data into independent sources. We then perform a separate localization procedure on each independent source. Because we localize sources independently, our method is just as reliable as single dipole source localization methods.

The steps of our method are depicted in Fig. 1. We begin by extracting the signal subspace of the EEG data using a Principal Component Analysis (PCA) algorithm. This step removes much of the noise from the data and reduces its dimensionality by truncating lower order terms of the decomposition (i.e., discarding the noise subspace). We then divide the PCA signal subspace into several components, using the recently developed Independent Component Analysis (ICA) [18], [19], [20] signal processing technique. The result of this preprocessing is a set of time-series signals (which sum to the original signal) at each electrode, where each time-series corresponds to an independent source in the model. The number of different maps created by ICA is equal to the number of temporally independent, stationary sources in the problem. To localize each of these independent sources, we solve a separate source localization problem. Specifically, for each independent component, we employ a downhill simplex search method [21] to determine the dipole which best accounts for that particular component's contribution of the signal.

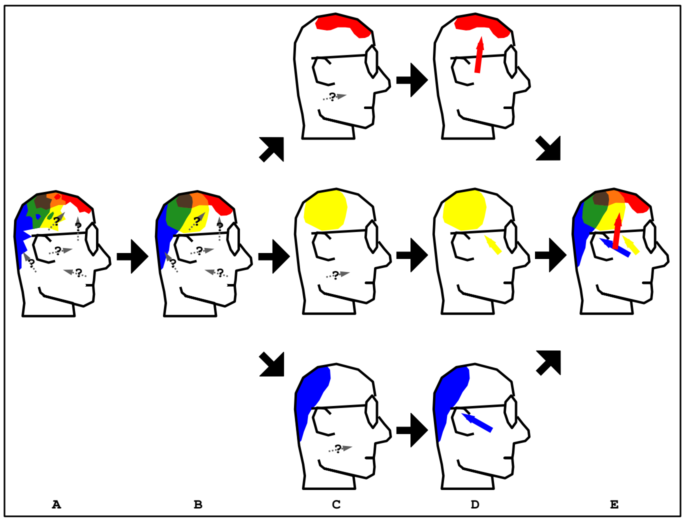

Fig. 1. A depiction of the steps of our algorithm. A) Measured signals are recorded at the scalp surface through EEG electrodes; the underlying neural sources (which we will model as dipoles) are unknown. B) With PCA decomposition, truncation, and reconstruction, much of the noise is removed from the EEG data. C) Using the ICA algorithm, the time signals can be decomposed into statistically independent activation maps (summing these activation maps returns the original measured signals). C) For each independent activation map, the single dipole source that best accounts for the map's voltages is localized. D) Integrated together, these independent dipole sources reproduce the signal from B).

In our study we use simulated data obtained by placing dipoles in a computational model at positions corresponding to observed epileptic sources in children with Landau-Kleffner syndrome [6]. We chose to simulate three tangential epileptogenic right-hemisphere sources, as shown in Fig. 2: the first in the temporal lobe, the second in the occipital lobe, and the third in the Sylvian fissure. This distributed configuration is typical of multifocal epilepsy, where each source has an independent time course [6]. For each of these sources, we use a time signal from a clinical study to its magnitude over time. That is, we place the three current dipoles inside our finite element model, and for each instant in time, we project the activation signals onto 32 clinically measured scalp electrode positions and add 2% noise to the signals. The electrode positions are shown in Fig. 3. Projecting the sources onto the electrodes requires the solution of a so-called *forward problem*.

Forward Problem

The EEG forward problem can be stated as follows: given the positions, orientations and magnitudes of dipole current sources, as well as the geometry and electrical conductivity of the head volume, Ω, calculate the distribu-

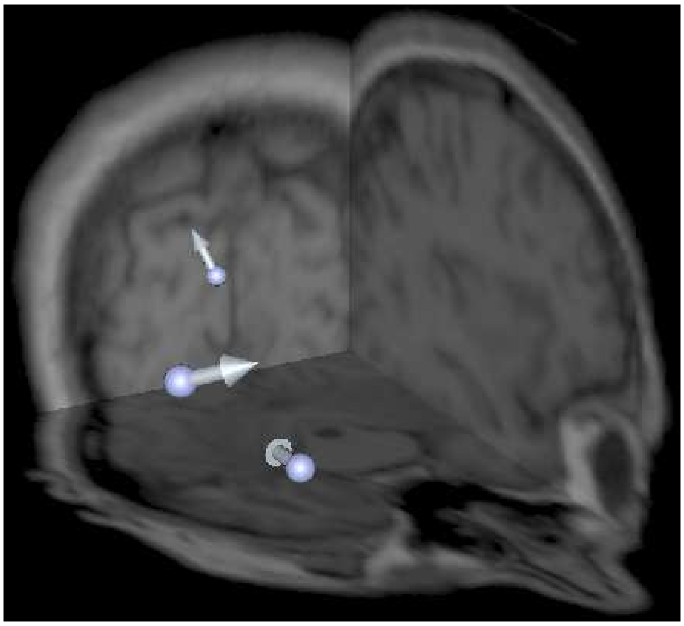

Fig. 2. Distribution of dipole sources (arrows) visualized with orthogonal MRI slices (background).

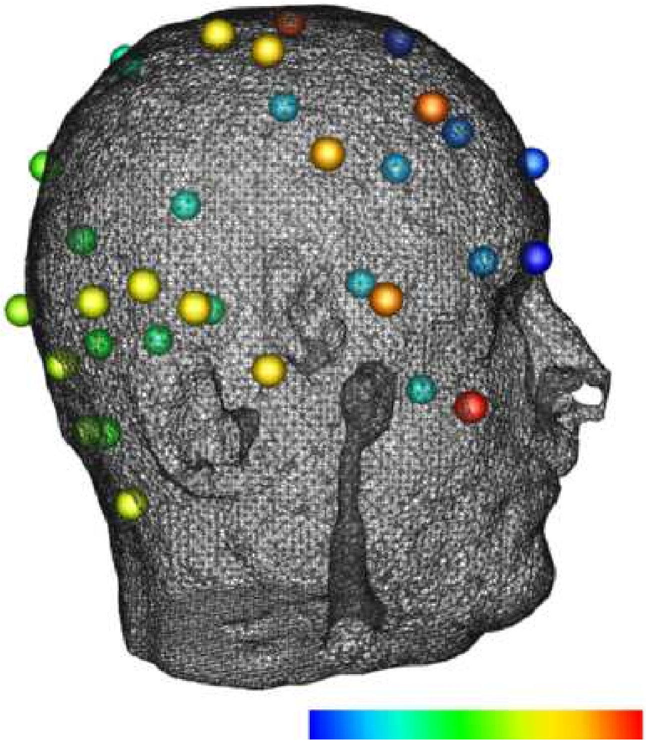

Fig. 3. Triangulated scalp surface with 32 electrodes. The electrodes have been color-mapped to indicate order: they are colored from blue to red as the channel number increases.

tion of the electric potential on the surface of the head (scalp), Γ_Ω. Mathematically, this problem can be described by Poisson's equation for electrical conduction in the head [22]:

$$\nabla \cdot (\sigma \nabla \Phi) = \sum I_s(\mathbf{r}), \quad \text{in} \quad \Omega \tag{1}$$

and Neumann boundary conditions on the scalp:

$$\sigma(\nabla \Phi) \cdot \mathbf{n} = 0, \quad \text{on} \quad \Gamma_\Omega \tag{2}$$

where σ is a conductivity tensor and I_s are the volume currents density due to current dipoles placed within the head. The unknown Φ is the electric potential created in the head by the distribution of current from the dipole sources. An ideal current dipole source can be described as two point sources of opposite polarity with infinitely large current density I_0 and infinitely small separation d:

$$I_s(\mathbf{r}) = \lim_{d \to 0} I_0[\delta(\mathbf{r} - \mathbf{r}_s - \frac{d}{2}) - \delta(\mathbf{r} - \mathbf{r}_s + \frac{d}{2})] \tag{3}$$

and $d \cdot I_0 = P$, the dipole strength.

To solve Poisson's equation numerically, we began with the construction of a computational model. The realistic head geometry was obtained from MRI data, where the volume was segmented and each tissue material was labeled in the underlying voxels [23]. The segmented head volume was then tetrahedralized via a mesh generator that preserved the classification when mapping from voxels to elements [24]. For each tissue classification, we assigned a conductivity tensor from the literature [25]. A cut-through of the classified mesh is shown in Fig. 4.

We then used the finite element method (FEM) to compute a solution within the entire volume domain [26]. The FEM allows us to capture the anisotropy of conductivity and accurate boundaries of the volume. The main idea behind the FEM is to reduce a continuous problem with infinitely many unknown field values to a finite number of unknowns by discretizing the solution region into elements. Then the values of the field at any point can be approximated by interpolation functions within every element in terms of the field values at specified points called nodes. Nodes are located at the element vertices where adjacent elements are connected. Details of the FEM method can be found in [26], [27], [28].

In our study, we use tetrahedral elements and linear interpolation functions within each tetrahedron. Our head model consists of approximately $768,000$ elements and $N = 164,000$ nodes. Once we have a geometric model, we can assemble the matrix equations (build the matrix $\mathbf{A}$) for relating field values at different nodes. This can be done using, for example, a Rayleigh-Ritz or Galerkin method [28]. Finally, we impose boundary conditions and apply source currents. These boundary and source conditions are incorporated within the right hand side (RHS) of the system (vector $\mathbf{b}$). As a result, when we move sources we do not have to rebuild the mesh or the matrix $\mathbf{A}$. We note that for linear interpolation functions, the RHS vector is not sensitive to the position of a source within an element; that is, for any position (though not orientation) within a particular tetrahedron, the contribution to the right hand side vector is the same. This ambiguity is relevant because

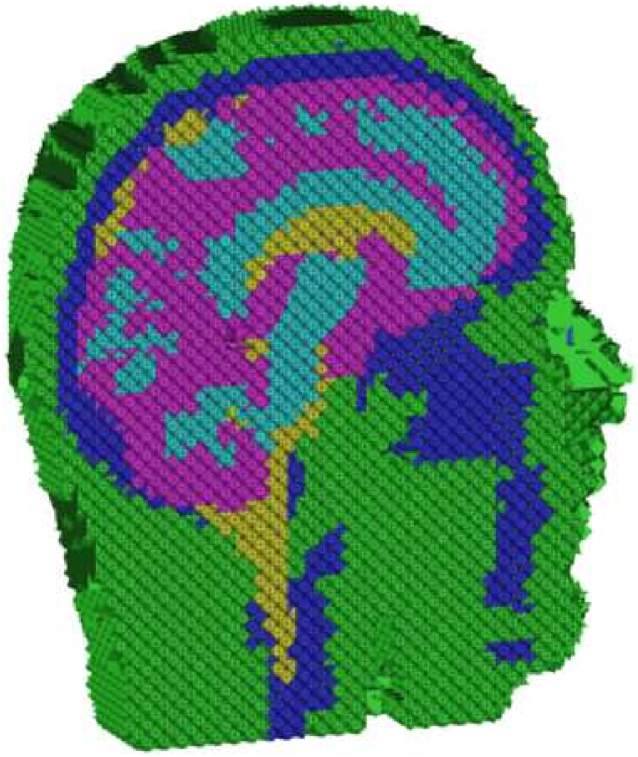

Fig. 4. Cut-through of the tetrahedral mesh, with elements colored according to conductivity classification. Green elements correspond to skin, blue to skull, yellow to cerebro-spinal fluid, purple to gray matter, and light blue to white matter.

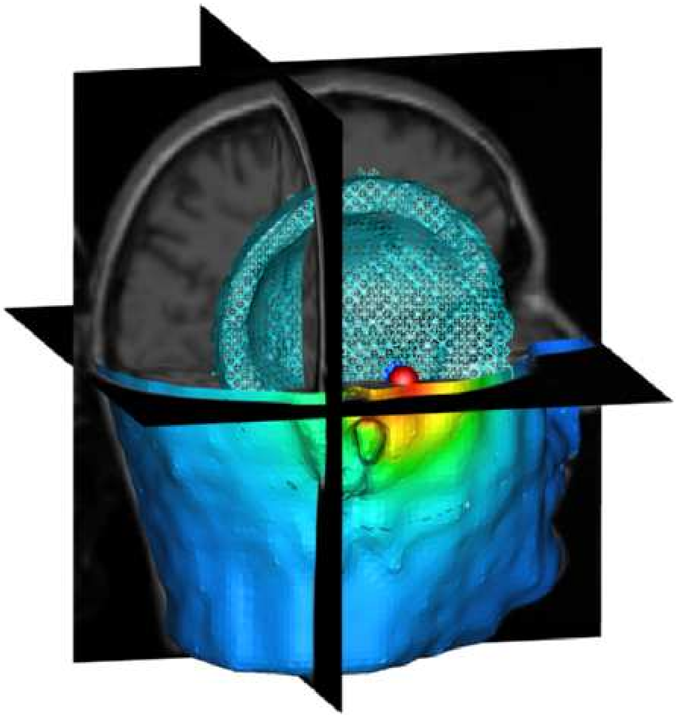

Fig. 5. Solution to a single dipole source forward problem. The underlying model is shown in the MRI planes, the dipole source is indicated with the red and blue spheres, and the electric field is visualized by a cropped scalp potential mapping and a wire-frame equipotential isosurface.

it will restrict the accuracy of our inverse solution when we attempt to recover the exact source positions.

Using the FEM, we obtain the linear system of equations:

$$\mathbf{A}_{ij}\Phi_j = \mathbf{b}_i \qquad (4)$$

where $\mathbf{A}_{ij}$ is an $N \times N$ stiffness matrix, $\mathbf{b}_i$ is a source vector and Φ_j is the vector of unknown potentials at the nodes within the head volume. The $\mathbf{A}$ matrix is sparse (containing approximately two million non-zeroes entries), symmetric, and positive definite.

The solution of this linear system was computed using a parallel conjugate gradient (CG) method and required approximately 12 seconds of wall-clock time on a 14 processor SGI Power Onyx with 195 MHz MIPS R10000 processors. The solution to a radially-oriented single dipole source forward problem is visualized in Fig. 5. In this image, we display an equipotential surface in wire frame, indicating the dipole location with red and blue spheres, cut-through the initial MRI data with orthogonal planes, and render the surface potential map of the bioelectric field on the cropped scalp surface.

In order to simulate time-dependent recordings, we first computed a forward solution due to each epileptic source, assuming dipoles of unit-strength. Each source produces a *map* of values at the simulated electrode sites. Running forward simulations for each of several dipoles results in a collection of several maps. To extend the single-instant values at the electrodes into time-dependent signals, we scaled the values of each map by pre-recorded clinical activation signals. Finally, we added 2% noise to the projected data to better simulate physical EEG measurements.

The above method for solving the forward problem is needed not only to derive the simulated electrode recordings, but also as the iterative engine for solving the inverse source localization problem.

Inverse Problem

The general EEG inverse problem can be stated as follows: given a set of electric potentials from discrete sites on the surface of the head and the associated positions of those measurements, as well as the geometry and conductivity of the different regions within the head, calculate the locations and magnitudes of the electric current sources within the brain.

Mathematically, it is an inverse source problem in terms of the primary electric current sources within the brain and can be described by the same Poisson's equation as the forward problem, Eq. (1), but with a different set of boundary conditions on the scalp:

$$\sigma(\nabla\Phi)\cdot\mathbf{n} = 0, \quad \text{and} \quad \Phi_j = \boldsymbol{\phi}_j \quad \text{on} \quad \Gamma_\Omega \qquad (5)$$

where $\boldsymbol{\phi}_j$ is the electrostatic potential on the surface of the head known at discrete points (electrode locations) and I_s in Eq. (1) are now unknown current sources.

The solution to this inverse problem can be formulated as the non-linear optimization problem of finding a least squares fit of a set of current dipoles to the observed data over the entire time series, or minimization with respect to the model parameters of the following cost function:

$$||\boldsymbol{\phi} - \hat{\boldsymbol{\phi}}|| = \sum_k \sum_{j=1}^{32} (\boldsymbol{\phi}_j(t_k) - \hat{\boldsymbol{\phi}}_j(t_k))^2 \tag{6}$$

where $\boldsymbol{\phi}_j(t_k)$ is the value of the measured electric potential on the j^{th} electrode at time instant t_k and $\hat{\boldsymbol{\phi}}_j(t_k)$ is the result of the forward model computation for a particular source configuration; the sum extends over all channels and time frames.

A brute-force implementation of the above method would require solving the forward problem for every possible configuration of dipoles in order to find the configuration that minimizes Eq. (6). Each dipole in the model has six parameters: location coordinates (x, y, z), orientation (θ, ϕ) and time-dependent dipole strength $P(t)$. The number of dipoles is usually determined by iteratively adding one dipole at a time until a "reasonable" fit to the data has been found. Even when restricting the location of the dipole to a lattice of sites, the configuration space is factorially large. This is a bottleneck of many localization procedures [12], [29].

Assume now that we could decompose the signals on the electrodes, such that we know electrode potentials due to each dipole *separately*. Then for every set of electrode potentials we would need to search for only one dipole, thus dramatically reducing our search space. We will discuss this useful filtering technique in the next section.

Statistical preprocessing of the data

In EEG experiments, electric potential is measured with an array of electrodes (typically 32, 64, or 128) positioned primarily on the top half of the head, as shown in Fig. 3. The data are typically sampled every millisecond during an interval of interest.

For a given electrode configuration, the time-dependent data can be arranged as a matrix, where every column corresponds to the sampled time frame and every row corresponds to a channel (electrode). For example, the data obtained by 32 electrodes in 180 ms can be sampled in 180 frames and represented as a matrix (32 × 180). Below we will refer to this matrix as $\boldsymbol{\phi}(t_k)$, where instead of a continuous variable t, we have sampled time frames t_k.

Before performing source localization, we will preprocess the EEG activation maps in order to decompose them into several *independent* activation maps. The source for each activation map will then be localized independently. This is accomplished as follows:

- First, we will process the raw signals, $\boldsymbol{\phi}(t_k)$, in order to reduce the dimensionality of the data, and to remove some of its noise. The projection of the data on the signal subspace will be referred to as $\boldsymbol{\phi}_s(t_k)$.
- The signal subspace, $\boldsymbol{\phi}_s(t_k)$, will then be decomposed into statistically independent terms, $\boldsymbol{\phi}_s^i(t_k)$.

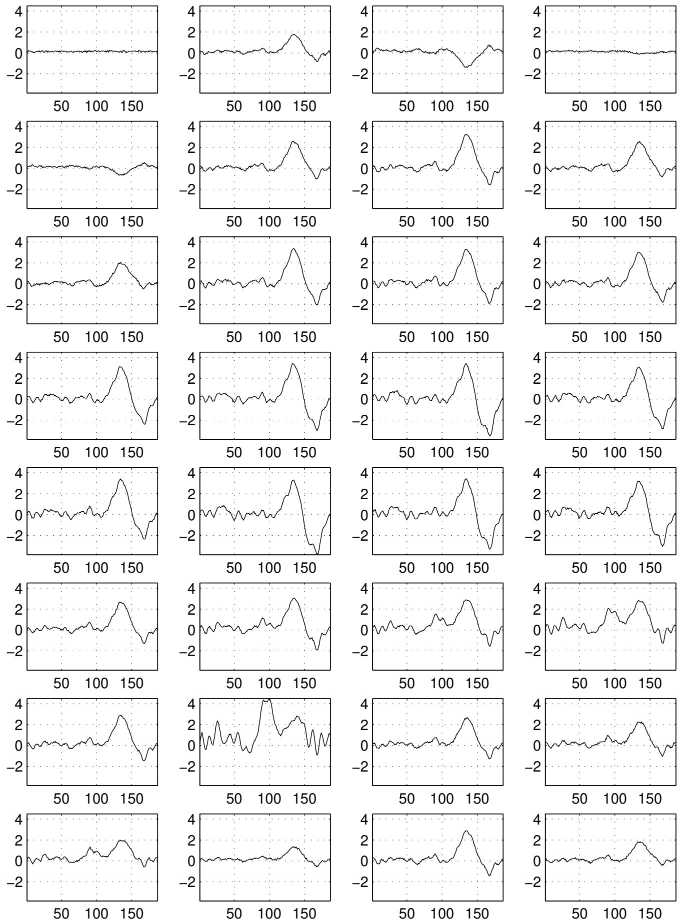

Fig. 6. Simulated scalp potentials due to three dipole sources mapped onto 32 channels (electrodes). Channels are numbered left to right, top to bottom. The first channel is the reference electrode. These signals are the input data for the ICA algorithm. The locations of these 32 electrodes are shown in Fig. 3.

- Each independent activation, $\boldsymbol{\phi}_s^i(t_k)$, will be assumed to be due to a single stationary dipole, which we will then localize using a parameterized search algorithm.

As outlined above, the first step in processing the raw EEG data, $\boldsymbol{\phi}(t_k)$, is to decompose the data into signal and noise subspaces by applying the Principal Component Analysis (PCA) method [30] (in the signal processing literature it is also known as the Karhunen-Loeve transform). The decomposition is achieved by finding the eigendecomposition of the data covariance matrix:

$$\mathbf{R} = E\{\boldsymbol{\phi}(t_k)\boldsymbol{\phi}^T(t_k)\} \approx \frac{1}{n}\sum_k \boldsymbol{\phi}_s(t_k) \cdot \boldsymbol{\phi}_s(t_k)^T \tag{7}$$

and constructing signal and noise subspaces [15]. The noise subspace will constitute the singular vectors with singular values less than a chosen noise threshold.

$$\mathbf{R} = \mathbf{U} \cdot \Lambda \cdot \mathbf{U}^T = \mathbf{U}_s \cdot \Lambda_s \cdot \mathbf{U}_s^T + \mathbf{U}_n \cdot \Lambda_n \cdot \mathbf{U}_n^T \tag{8}$$

Having constructed the subspaces, we can project the original data onto the signal subspace by:

$$\boldsymbol{\phi}_s(t_k) = \sqrt{\Lambda_s}^{(-1)} \cdot \mathbf{U}_s^T \cdot \boldsymbol{\phi}(t_k) \tag{9}$$

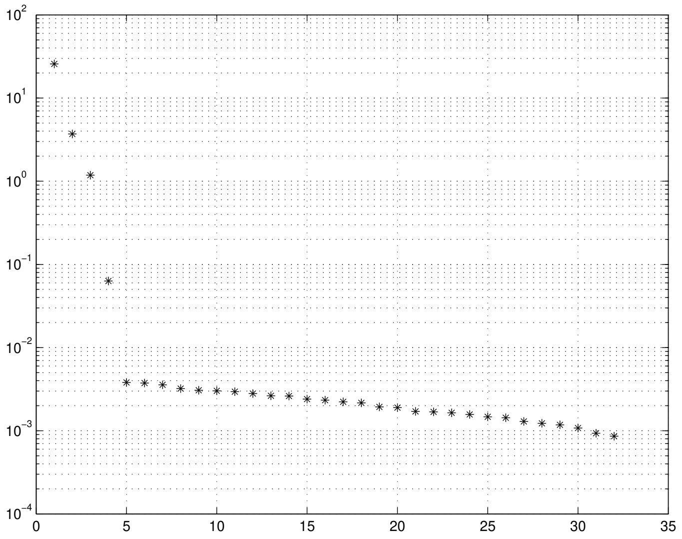

Fig. 7. Singular values of the covariance matrix. It appears that only the first four singular values contribute to the signal subspace, with the rest constituting the noise subspace.

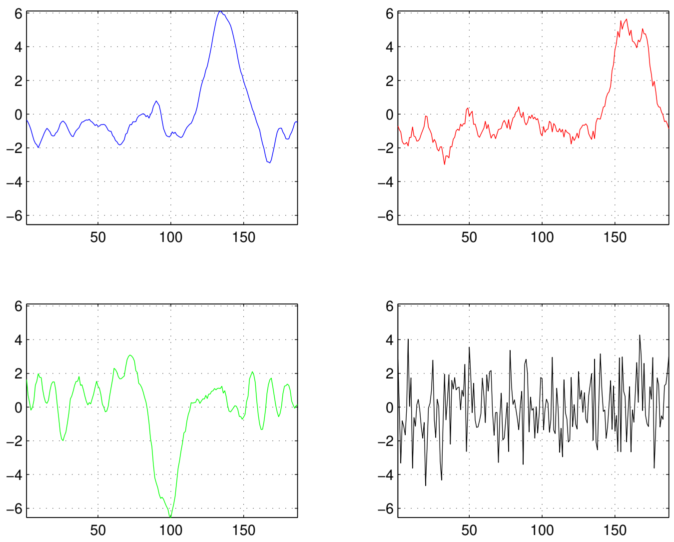

Fig. 8. ICA activation maps obtained by unmixing the signals from the signal subspace. We observe that there are only three independent patterns, indicating the presence of only three separate signals in the original data; the fourth component is noise.

where Λ_s and $\mathbf{U}_s$ are the signal subspace singular values and singular vectors.

Though PCA allows us to estimate the number of dipoles, in the presence of noise it does not necessarily give an accurate result [15]. In order to separate out any remaining noise, as well as each statistically independent term, we will use the recently derived *infomax* technique, Independent Component Analysis (ICA). (It is worth noting that PCA not only filters out noise from the data, but also makes a preliminary step of ICA decomposition by decorrelating the channels, or removing *linear* dependence, i.e., $E\{\mathbf{s}_i \cdot \mathbf{s}_j\} = 0$. ICA then makes the channels *independent*, i.e., $E\{\mathbf{s}_i^n \cdot \mathbf{s}_j^m\} = 0$ for any powers n and m.)

There are several assumptions one needs to make about the sources in order to apply the ICA algorithm in electroencephalography [19]:

- the sources must be independent (signals come from statistically independent brain processes);[2]
- there is no delay in signal propagation from the sources to the detectors (conducting media without delays at source frequencies);
- the mixture is linear (Poisson's equation is linear);
- the number of independent signal sources does not exceed the number of electrodes (we expect to have fewer strong sources than our 32 electrodes).

It follows then that since the PCA-processed EEG recordings $\boldsymbol{\phi}_s(t_k)$ are the result of linear combinations of the source signals $\mathbf{s}(t_k)$, they can therefore be expressed as:

$$\boldsymbol{\phi}_s(t_k) = \mathbf{M} \cdot \mathbf{s}(t_k), \tag{10}$$

where $\mathbf{M}$ is the so-called "mixing" matrix and each row of $\mathbf{s}(t_k)$ is a source's time activation. What we would like to find is an "unmixing" matrix $\mathbf{W}$, such that:

$$\mathbf{W} \cdot \boldsymbol{\phi}_s(t_k) = \mathbf{W} \cdot \mathbf{M} \cdot \mathbf{s}(t_k) = \mathbf{s}(t_k), \tag{11}$$

or, in other words, $\mathbf{W} = \mathbf{M}^{-1}$; but we do not know $\mathbf{M}$, the only data we have is the $\boldsymbol{\phi}_s(t_k)$ matrix.

Under the assumption of *independent* sources, ICA allows us to construct such a $\mathbf{W}$ matrix; however, since neither the matrix nor the sources are known, $\mathbf{W}$ can be restored only up to scaling and permutations (i.e., $\mathbf{W} \cdot \mathbf{M}$ is not an identity matrix, but rather is equal to $\mathbf{S} \cdot \mathbf{P}$, where $\mathbf{S}$ is a diagonal scaling matrix and $\mathbf{P}$ is a permutation matrix). This problem is often referred to as Blind Source Separation (BSS) [18], [31], [32], [33].

The ICA process consists of two phases: the learning phase and the processing phase. During the learning phase, the ICA algorithm finds a weighting matrix $\mathbf{W}$, which minimizes the mutual information between channels (variables), i.e., makes output signals that are statistically independent in the sense that the multivariate probability density function of the input signals becomes equal to the product of $f_{\mathbf{u}} = \prod_i f_{\mathbf{u_i}}(\mathbf{u_i})$ probability density functions (p.d.f.) of every independent variable. This is equivalent to maximizing the entropy of a non-linearly transformed vector $\mathbf{u} = \mathbf{g}(\mathbf{W}\boldsymbol{\phi}_s)$:

$$H(\mathbf{u}) = -E\{log f_u(\mathbf{u})\} = -\int f_u(\mathbf{u}) log f_u(\mathbf{u}) d\mathbf{u} \tag{12}$$

where $\mathbf{g}$ is some non-linear function.

There exist several different ways to estimate the $\mathbf{W}$ matrix. For example, the Bell-Sejnowski infomax algorithm [18] uses weights that are changed according to the entropy gradient. Below, we use a modification of this rule as proposed by Amari, Cichocki and Yang [20], which uses the natural gradient rather than the absolute gradient of

[2]We note that this assumption is thought to be valid for our multifocal epilepsy source localization problem; however, it may not be valid for other neural events.

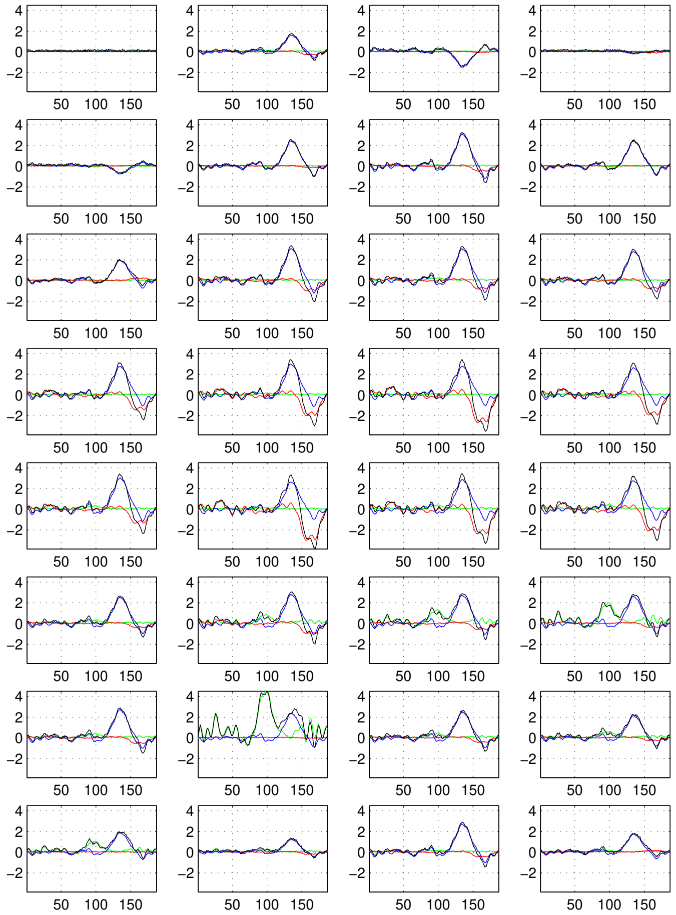

Fig. 9. The projection of the first three activation maps from Fig. 8 (as well as the original signals from Fig. 7) onto the 32 electrodes.

$H(\mathbf{u})$. This allows us to avoid computing matrix inverses and to speed up solution convergence:

$$\mathbf{W}_{k+1} = \mathbf{W}_k + \mu_k \cdot [\mathbf{I} + 2g(\mathbf{y}_k) \cdot \mathbf{y}_k^T] \cdot \mathbf{W}_k \qquad (13)$$

where the vector $\mathbf{y}$ is defined as:

$$\mathbf{y}_k = \mathbf{W}_k \cdot \boldsymbol{\phi}_s(t_k) \qquad (14)$$

and for the nonlinear function g we used:

$$g(\mathbf{y}_k) = tanh(\mathbf{y}_k) \qquad (15)$$

In the above equation μ_k is a learning rate and $\mathbf{I}$ is the identity matrix [33]. The learning rate decreases during the iterations and we stop when μ_k becomes smaller than a pre-defined tolerance (e.g., 10^{-6}).

The second phase of the ICA algorithm is the actual source separation. Independent components (activations) can be computed by applying the unmixing matrix $\mathbf{W}$ to the signal subspace data:

$$\mathbf{s}(t_k) = \mathbf{W} \cdot \boldsymbol{\phi}_s(t_k) \qquad (16)$$

Projection of independent activation maps $\mathbf{s}(t_k)$ back onto the electrodes one at a time can be done by:

$$\boldsymbol{\phi}^i(t_k) = \mathbf{U}_s \cdot \sqrt{\Lambda} \cdot \mathbf{W}^{(-1)} \cdot \mathbf{s}_i(t_k) \qquad (17)$$

where $\boldsymbol{\phi}^i(t_k)$ is the set of scalp potentials due to just the i^{th} source. For $\mathbf{s}_i(t_k)$ we zero out all rows but the i^{th}; that is, all but the i^{th} source are "turned off". In practice we will not need the full time sequence $\boldsymbol{\phi}^i(t_k)$ in order to localize source $\mathbf{s}_i$, but rather simply a single instant of activation. For this purpose, we set the $\mathbf{s}_i$ terms to be unit sources (i.e., $\mathbf{s} = \mathbf{I}$), resulting in $\boldsymbol{\phi}^i$ row elements which are simply the corresponding columns of $\mathbf{U}_s \cdot \sqrt{\Lambda} \cdot \mathbf{W}^{(-1)}$.

Source localization

For each electrode potential map $\boldsymbol{\phi}^i$, we can now localize a single dipole using a search method to minimize Eq. (6). We have chosen to use the straight-forward downhill simplex search. Since we know we are only searching for one dipole source which produced each activation map, $\boldsymbol{\phi}^i$, we will only need to optimize six degrees of freedom: the position (x, y, z), orientation (θ, ϕ) and strength P of a single dipole. The last three variables can be thought of as components (p_x, p_y, p_z), the dipole strength in the x, y and z direction.

Since the potential is a linear function of dipole moment, we can further reduce our search space by using the analytic optimization from [34], [35]. Specifically, for each location to be evaluated for the simplex, we separately compute the solutions due to dipoles oriented in the x, y and z directions, and solve a 3×3 system to determine the optimal strength and orientation for that position [37]. The minimization cost function now explicitly depends on only the coordinates of the dipole

$$R(x, y, z) = ||\boldsymbol{\phi}^i - \bar{p_x}\hat{\boldsymbol{\phi}}_x - \bar{p_y}\hat{\boldsymbol{\phi}}_y - \bar{p_z}\hat{\boldsymbol{\phi}}_z|| \qquad (18)$$

To perform non-linear minimization of $R(x, y, z)$, we applied the multi-start downhill simplex method [21], [36], as implemented in [38]. In an N-dimensional space, the simplex is a geometric figure that consists of N+1 fully interconnected vertices. In our case we are searching a three-dimensional coordinate space, so the simplex is just a tetrahedron with four vertices. The downhill simplex method searches for the minimum of the three-dimensional function by taking a series of steps, each time moving a point in the simplex (a dipole) away from where the function is largest (see Fig. 10).

The single dipole solution to the source localization problem is unique [39]. This follows from the fundamental physical properties of the model and can be illustrated by considering the cost function Eq. (6) over its entire three-dimensional domain. A computationally efficient method for evaluating the cost function using lead-field theory is discussed in [37]. However, despite the uniqueness of the solution, in the case of linear finite elements the downhill simplex search method may fail to reach the global minimum. This can happen when the nodes of the simplex (and its attempted extensions) are all contained within a single element of the finite element model. In such situations, the simplex must be restarted several times in order to find the true global minimum.

After all of the dipoles have been localized, the only step which remains is to determine their absolute strengths.

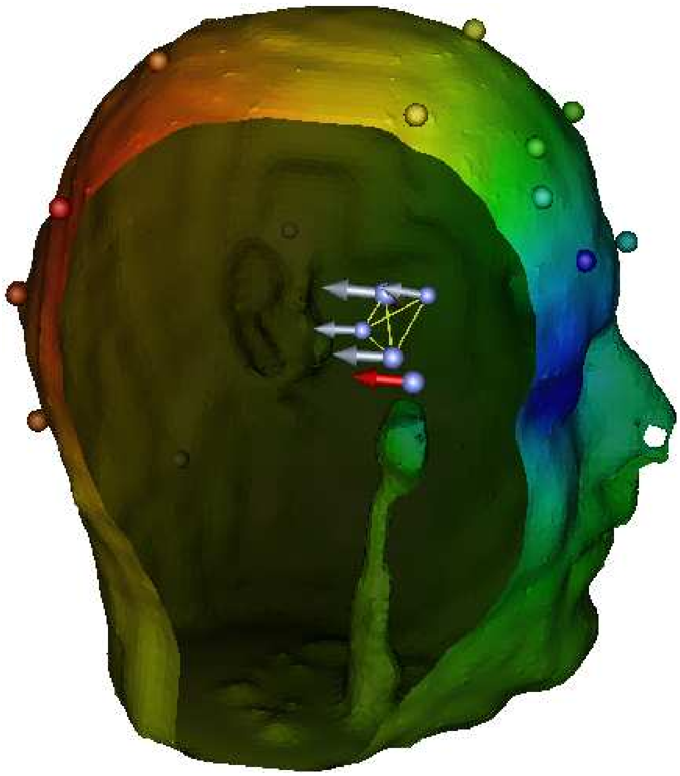

Fig. 10. Visualization of the downhill simplex algorithm converging to a dipole source. The simplex is indicated by the gray vectors joined by yellow lines. The true source is indicated in red. The surface potential map on the scalp is due to the forward solution of one of the simplex vertices, whereas the potentials at the electrodes (shown as small spheres) are the "measured" EEG values (potentials due to the true source).

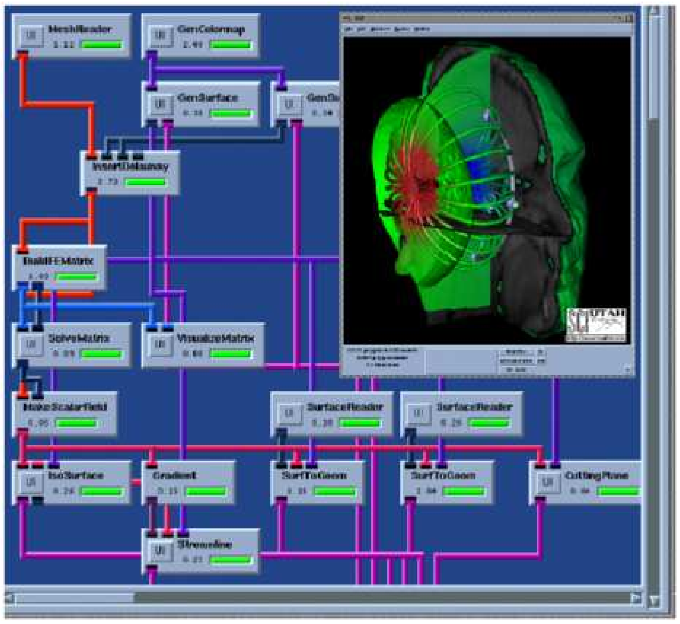

Fig. 11. The SCIRun problem solving environment. The user can select physiologically plausible regions of the model in which to seed the downhill simplex algorithm, thereby steering the algorithm to a more rapid convergence.

This can be accomplished by solving a small, $m\times m$, linear minimization problem, where m is the number of dipoles. For this study, we recovered three dipoles, so we solved a 3×3 system, where the right hand side is formed by the inner products of optimized single dipole solutions and EEG recordings $\hat{\boldsymbol{\phi}}$.

An Inverse EEG Problem Solving Environment

One of the challenges of solving the inverse EEG source localization problem is choosing initial configurations for the downhill simplex solver. A good choice can result in rapid convergence, whereas a bad choice can cause the algorithm to search somewhat randomly for a very long time before closing in on the solution. Furthermore, because the solution space has many plateaus due to the linear finite element model, it is generally necessary to re-seed the algorithm multiple times in order to find the global minimum.

We have brought the user into the loop by enabling seed-point selection within the model. The user can seed specifically within physiologically plausible regions. This focus enables the algorithm to converge much more quickly, rather than repeatedly wandering through non-interesting regions.

To steer our algorithm, we utilized the SCIRun problem solving environment [40]. SCIRun is a scientific programming environment that allows the interactive construction, debugging, and steering of large-scale scientific computations. SCIRun can be envisioned as a "computational workbench," in which a scientist can design and modify simulations interactively via a dataflow programming model. As opposed to the typical "off-line" simulation mode (in which the scientist manually sets input parameters, computes results, visualizes the results via a separate visualization package, and then starts again at the beginning), SCIRun "closes the loop" and allows interactive steering of the design, computation, and visualization phases of a simulation. The images of our algorithm running within the SCIRun environment are shown in Fig. 10 and Fig. 11.

Numerical Simulations

We prepared the simulated data as described in the previous sections. The time-dependent course of 180 ms for all 32 channels is shown in Fig. 6. We also provide a color mapped plot of the potentials on the surface of the head for the time step at 160 ms (maximum variance) in Fig. 12. As can be seen in the latter figure, the distribution of potentials on the scalp can hardly be attributed to a single dipole, but rather to a configuration of several dipoles. We perform PCA on the original EEG time-dependent data and the singular values are shown in Fig.7. Analyzing the singular values, we can deduce that the signal subspace consists of the four first singular vectors. Working with just the contribution of these four components Eq. (9), we perform the ICA procedure, resulting in the activation maps shown in Fig. 8. Notice that there are only three different activation patterns presented; the fourth component is

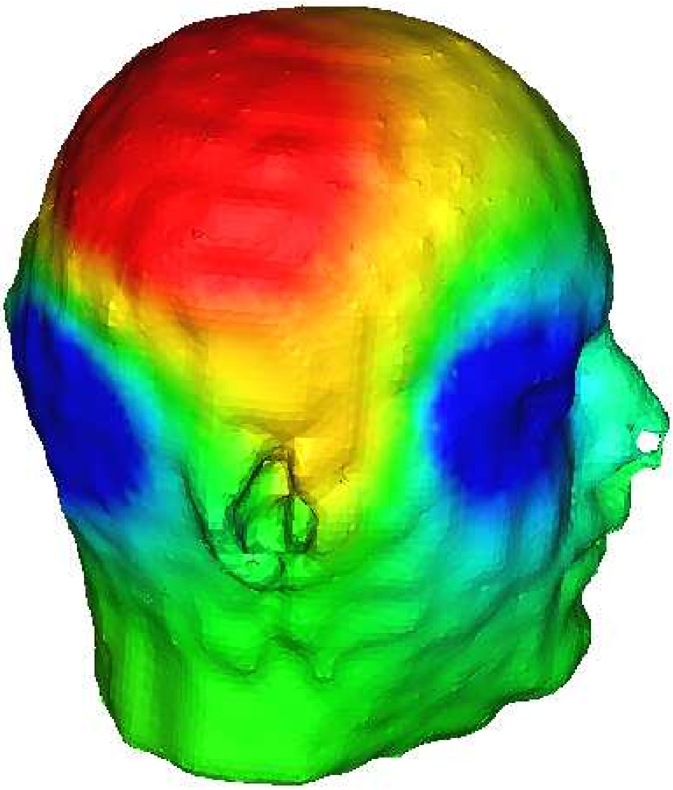

Fig. 12. Scalp surface potential map due to several dipoles, corresponding to time T=160 ms from the signals shown in Fig. 6.

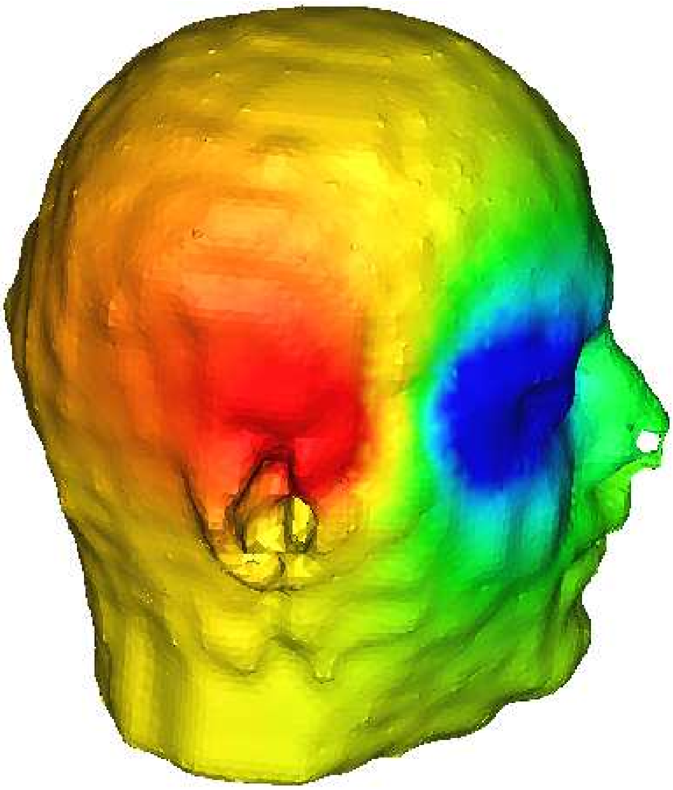

Fig. 13. Projection of the first ICA component onto the 32 channels at the time T = 160 ms.

actually just noise.

Projecting the first activation back onto all 32 channels, we get the signals shown in Fig. 9, which are the potentials due to the single temporal lobe dipole. Plotting the potentials again for the time step at 160 ms in Fig. 13, one can recognize the surface potential map as resulting from the activation of a single dipole source. This is evidenced by the well-defined foci near the right eye and ear, as well as the symmetric potential fall-off about the dipole plane.

We can check the accuracy of the ICA decomposition by comparing the above results to the results of the forward simulation run with the two other dipoles "turned off". Because ICA does not preserve scale, we use time-space correlation coefficients as our metric for comparing the potentials at the electrodes. The sets of electrode potentials are viewed as vectors in time-space and the cosine of the "angle" between them is calculated by taking the dot-product of the two vectors after they have been normalized. Evaluated this way, our three activation projections restored the original (unmixed) potential distribution with RMS errors of 2%, 3% and 5%.

We now turn our attention to the last step of the procedure: source localization. For our head model, on average, the downhill simplex algorithm required only $2-3$ interactive restarts in order to converge to the correct solution, with an average run of $30-50$ iterations. This is a substantial speed-up compared to the batch-mode multi-start multiple dipole localization methods reported in [36]. The localized temporal lobe dipole was found to be accurate within 4 mm of the actual source. We repeated this localization procedure for the occipital lobe and Sylvian fissure dipoles and were able to determine their positions with errors of 5 and 2 mm, respectively.

Conclusions

We have presented an algorithm that reduces the complexity of localizing multiple neural sources by exploiting the time dependence of the data. We have shown that on a realistic head model with simulated EEG data, our algorithm is capable of correctly predicting the number of independent sources in the model and reconstructing potentials due to each source separately. These potential maps can be successfully used by source localization methods to independently localize sources.

By integrating our algorithm within the SCIRun problem solving environment, we were able to computationally steer the multi-start downhill simplex algorithm towards probable regions of activation. Interactive control of the simulation, coupled with statistical data preprocessing of the data enabled us to dramatically increase the efficiency and accuracy of recovering multiple sources from EEG data.

I. Acknowledgments

This work was supported in part by the National Science Foundation, the Department of Energy, the National Institutes of Health and the Utah State Centers of Excellence Program.

References

[1] **Gulrajani RM:** *Bioelectricity and Biomagnetism*, John Wiley and Sons, 1998.

[2] **Hadamard J:** Sur les problemes aux derivees parielies et leur signification physique. *Bull Univ of Princeton* 49-52, 1902.

[3] **Nunez PL:** *Electric Fields of The Brain*, New York: Oxford, 1981.

[4] **Koles ZJ:** Trends in EEG source localization. *Electroencephalography and clinical Neurophysiology* 106: 127-137, 1998.

[5] **Huiskamp GGM, Maintz JBA, Wieneke GH, Viergever VA, van Huffelen AC:** The influence of the use of realistic head geometry in the dipole localization of interictal spike activity in MTLE patients. *NFSI* 97: 84-87, 1997.

[6] **Paetau R, Granstrom M, Blomstedt G, Jousmaki V, Korkman M, et al.,:** Magnetoencephalography in presurgical evaluation of children with Landau-Kleffner syndrome. *Epilepcia* 40: 326-335, 1999.

[7] **Rush S, Driscoll DA:** EEG electrode sensitivity - an application of reciprocity. *IEEE Trans Biomed Eng* 16: 15-22, 1969.

[8] **Smith DB, Sidman RD, Flanigin H, Henke J, Labiner D:** A reliable method for localizing deep intracranial sources of the EEG. *Neurology* 35: 1702-1707, 1985.

[9] **Roth BJ, Balish M, Gorbach A, Sato S:** How well does a three-sphere model predict positions of dipoles in a realistically shaped head? *Electroencephalography and clinical Neurophysiology* 87: 175-184, 1993.

[10] **Gorodnitsky IF, George JS, Rao BD:** Neuromagnetic source imaging with FOCUSS: a recursive weighted minimum norm algorithm. *Electroencephalography and clinical Neurophysiology* 95: 231-251, 1995.

[11] **Pascual-Marqui RD, Michel CM, Lehnam D:** Low resolution electromagnetic tomography: A new method for localizing electrical activity in the brain. *International Journal of Psychophysiology* 18: 49-65, 1994.

[12] **Supek S, Aine CJ:** Simulation studies of multiple dipole neuromagnetic source localization: model order and limits of source resolution. *IEEE Trans Biomed Eng* 40: 354-361, 1993.

[13] **Achim A, Richer F, Saint-Hilaire:** Methods for separating temporally overlapping sources of neuroelectric data. *Brain topography* 1: 22-28, 1988.

[14] **Scherg M, von Cramon D:** Two bilateral sources of the late AEP as identified by a spatio-temporal dipole model. *Electroenceph Clin Neurophysiol* 62: 290-299, 1985.

[15] **Mosher JC, Lewis PS, Leahy RM:** Multiple dipole modeling and localization from spatio-temporal MEG data. *IEEE Trans Biomed Eng* 39: 541-57, 1992.

[16] **Mosher JC, Leahy RM:** EEG and MEG source localization using recursively applied (RAP) MUSIC. *Los Alamos National Laboratory Report* LA-UR-96-3889.

[17] **Cuffin BN:** EEG dipole source localization *IEEE Engineering in Medicine and Biology* 17: 118-122, 1998.

[18] **Bell AJ, Sejnowski TJ:** An information-maximization approach to blind separation and blind deconvolution. *Neural Computation* 7: 1129-1159, 1995.

[19] **Makeig S, Bell AJ, Jung T-P, Sejnowski TJ:** Independent Component Analysis of Electroencephalographic data. *Advances in Neural Information Processing Systems* 8: 145-151, 1996.

[20] **Amari S, Cichocki A, Yang HH:** A new learning algorithm for blind signal separation. *Advances in Neural Information Processing Systems* 8, 1996.

[21] **Nedler JA, Mead R:** A simplex method for function minimization. *Compt J* 7: 308-313, 1965.

[22] **Plonsey R:** Volume Conductor Theory, *The Biomedical Engineering Handbook.* Bronzino JD, editor, 119-125, CRC Press, Boca Raton, 1995.

[23] **Wells WM, Grimson WEL, Kikinis R, Jolesz FA:** Statistical intensity correction and segmentation of MRI data. *Visualization in Biomedical Computing*: 13-24, 1994.

[24] **Schmidt JA, Johnson CR, Eason JC, MacLeod RS:** Applications of automatic mesh generation and adaptive methods in computational medicine. *Modeling, Mesh Generation, and Adaptive Methods for Partial Differential Equations*, Babuska I et al.,editors, Springer-Verlag, 367-390, 1995.

[25] **Foster KR, Schwan HP:** Dielectric properties of tissues and biological materials: A critical review. *Critical Reviews in Biomed. Eng.* 17: 25-104, 1989.

[26] **Miller CE, Henriquez CS:** Finite Element Analysis of bioelectric phenomena. *Critical Reviews in Biomed. Eng.* 18: 181-205, 1990.

[27] **Yan Y, Nunez PL, Hart RT:** Finite-element model of the human head: scalp potentials due to dipole sources. *Med Biol Eng Comp* 29: 475-481, 1991.

[28] **Jin J:** *The Finite Element Method in Electromagnetics*, John Wiley and Sons, 1993.

[29] **Harrison RR, Aine CJ, Chen H-W, Flynn ER, Huang M:** Investigation of Methods for Spatiotemporal Neuromagnetic Source Localization. *Los Alamos National Laboratory Report* LA-UR-96-2042.

[30] **Glaser EM, Ruchkin DS :** *Principles of Neurobiological Signal Analysis*, Chapter 5, New York: Academic, 1976.

[31] **Jutten C, Herald J:** Blind separation of sources, part I: an adaptive algorithm based on neurometric architecture. *Signal Processing* 24: 1-10, 1991.

[32] **Comon P:** Independent component analysis, a new concept? *Signal Processing* 36: 287-314, 1994.

[33] **Makeig S, Jung T-P, Bell AJ, Ghahremani D, Sejnowski TJ:** Blind separation of event-related brain responses into Independent Components, *Proc Natl Acad Sci* USA, 1997.

[34] **Awada KA, Jackson DR, Williams JT, Wilton DR, Baumann SB, Papanicolaou AC:** Computational aspects of finite element modeling in EEG source localization. *IEEE Trans Biomed Eng* 44: 736-752, 1997.

[35] **Salu Y, Cohen LG, Rose D, Sato S, Kufta C, Hallett M:** An improved method for localizing electric brain dipoles. *IEEE Trans Biomed Eng* 37: 699-705, 1990.

[36] **Huang M, Aine CJ, Flynn ER:** Multi-start Downhill Simplex Method for Spatio-temporal Source Localization in Magnetoencephalography. *Electroencephalography and clinical Neurophysiology* 108: 32, 1998.

[37] **Zhukov LE and Weinstein DW:** Lead field basis for FEM source localization. *University of Utah Technical Report* UUCS-99-014.

[38] **Press WH, Teukolsky SA, Vetterling WT, Flannery BP:** *Numerical Recipes in C*, Cambridge University Press, 1992.

[39] **Amir A:** Uniqueness of the generators of brain evoked potential maps *IEEE Trans Biomed Eng* 41: 1-11, 1994.

[40] **Parker SG, Weinstein DM, Johnson CR:** The SCIRun computational steering software system. In E. Arge, A.M. Bruaset, and H.P. Langtangen, editors, *Modern Software Tools in Scientific Computing*, 1-44, Birkhauser Press, 1997.